

# Effect of surface anisotropy on the magnetic properties of magnetite nanoparticles: A Heisenberg-Monte Carlo study

J. Mazo-Zuluaga <sup>a)</sup> and J. Restrepo

*Grupo de Estado Sólido,*

*Grupo de Instrumentación Científica y Microelectrónica*

*Instituto de Física,*

*Universidad de Antioquia. A.A. 1226,*

*Medellín, Colombia*

J. Mejía-López

*Facultad de Física,*

*Pontificia Universidad Católica,*

*Av. Vicuña Mackenna 4860,*

*Santiago, Chile*

(Dated: March 26, 2008)

## Abstract

In this study we analyze the effect of surface anisotropy on the magnetic properties of magnetite  $\text{Fe}_3\text{O}_4$  nanoparticles on the basis of a core-shell model. Magnetization, magnetic susceptibility and specific heat are computed over a wide range of temperatures. In our model, we stress on magnetite nanoparticles of 5 nm in diameter which consist of 6335 ions. Our theoretical framework is based on a three-dimensional classical Heisenberg Hamiltonian with nearest magnetic neighbors interactions between iron ions involving tetrahedral ( $A$ ) and octahedral ( $B$ ) sites. Terms dealing with cubic magnetocrystalline anisotropy for core ions, a single-ion site surface anisotropy for those Fe ions belonging to the shell, and the interaction with a uniform external magnetic field are considered. To compute the equilibrium averages, a single-spin movement Monte Carlo-Metropolis dynamics was used. Results reveal the occurrence of low-temperature spin configurations different from those expected for a collinear single-domain ferrimagnetic state, depending on the magnitude and sign of the surface anisotropy constant. A transition to a spike state, with magnetization close to zero, is obtained beyond certain critical positive surface anisotropy value. Such a transition is not observed for negative values. Moreover, a two-pole magnetic state is developed at sufficiently high negative values. Such differences are explained in terms of the interplay between the superexchange couplings and the easy directions imposed by the surface anisotropy vectors. Our results are summarized in a proposal of phase diagram for the different spin structures as a function of the surface-to-core anisotropy ratio. Lastly, hysteretic behavior is evaluated. Nanoparticles become magnetically harder as the surface anisotropy increases in magnitude, and the way in which the coercive field changes with this quantity is explicitly shown.

<sup>a)</sup> Electronic mail: [jomazo@fisica.udea.edu.co](mailto:jomazo@fisica.udea.edu.co)

## I. INTRODUCTION

As is well established, magnetic properties in nanoparticles are different from those found in bulk systems and are strongly influenced by finite size effects and the breaking of crystal symmetry at the surface. In consequence, nanoparticles are characterized by having reduced coordination, roughness, broken exchange bonds, local structural disorder, defects, uncompensated spins, a large surface-to-volume ratio [1–5], etc.

Such effects are more pronounced as the particle size diminishes. Among these effects, experimental evidence endorsing both the occurrence of surface spin disorder and the idea of a core-shell model can be found in the literature on this topic. For instance, spin canting in  $\text{NiFe}_2\text{O}_4$  [1] and  $\gamma\text{-Fe}_2\text{O}_3$  [2] nanoparticles was proposed as the mechanism responsible for moment reduction. Polarized neutron scattering experiments on  $\text{CoFe}_2\text{O}_4$  nanoparticles were consistent with a core of aligned spins surrounded by a magnetically disordered shell [3]. Hence, the scenario of a state where surface spins become canted and oriented in directions different from those ruled out by internal magnetocrystalline anisotropy has been postulated. The same idea was concluded for both chemically precipitated [4] and ball-milled  $\text{NiFe}_2\text{O}_4$  nanoparticles [5]. In this last study, the authors even proposed that the canted spins on the surface freeze into a spin-glass-like state below a freezing temperature at around 50 K. For magnetite, which is an iron ferrite  $\text{FeFe}_2\text{O}_4$ , and in general for any ferrimagnetic ferrite nanoparticle, there are several reasons for expecting surface spin disorder. Among them, we could mention variations in surface cations coordination, absence of oxygen ions at or near the surface giving rise to broken bonds, gradients in the superexchange integrals due to relaxed positions of surface cations, which in turn induce changes in the magnetocrystalline anisotropy, etc. Another important feature is the coating medium or the matrix in which nanoparticles are embedded. Regarding the influence of coating medium, a recent effort to understand the effect of having different surfactant coatings on the magnetic properties of  $\text{Fe}_3\text{O}_4$  nanoparticles by means of electronic spin resonance (ESR) was carried out by Koseoglu [6]. Here, nanoparticles were coated with gold, Na-oleate and methoxypolyethylene glycol. The results showed differences in the resonance fields and linewidth of the ESR spectra indicating strong magnetic surface effects depending on the coating employed. In particular, surface effects are enhanced by gold coating due to strong interactions between gold atoms and cations on the surface.

As to the role of the surface anisotropy constant on the magnetic properties in nanoparticles, and its magnitude compared to the bulk constants, some interesting results have also been reported. For instance, the persistence of hysteresis up to values as large as 160 kOe in ball-milled  $\text{NiFe}_2\text{O}_4$  nanoparticles at 4.2 K was interpreted as resulting from surface anisotropy fields 400 times larger than the bulk magnetocrystalline anisotropy field [5]. Moreover, giant anisotropy has been shown to occur in thiol-capped gold nanoparticles [7]. Here, a diamagnetic system is able to exhibit magnetic hysteresis as a result of the interplay between surface Au atoms and the localized holes formed in the  $5d$  band by the thiol ligands on the surface, giving rise to a very high local surface anisotropy. In this system, a value of the anisotropy constant greater than  $7 \times 10^7 \text{ J/m}^3$  was reported. This enormous value is larger than that corresponding to typical highly anisotropic systems such as hexagonal  $\text{SmCo}_5$ .

Additionally, several simulation-based works show the influence of a surface anisotropy constant larger than that of the core, even several orders of magnitude larger, on the hysteretic behavior and magnetic properties of nanoparticles [8–13]. Other simulation studies concerning the effect of surface anisotropy in nanoparticles have also been reported by different authors [14–17]. Nevertheless, a deeper insight into understanding such behaviors is called for. Finally, despite the fact that magnetite is one of the best known and studied iron oxides, it has very recently attracted considerable interest. The most recent issues range from the use of magnetite nanoparticles to emulate the magnetic properties of human brain tissue [18], three-dimensional arrays of magnetite nanoparticles to manufacture magneto-electronic devices [19], and ferrofluids [20], to biocompatible nanoparticles for hyperthermia [21] and nanoparticles loaded with Indomethacin as an anti-inflammatory drug for magnetic drug targeting [22], among many other studies dealing both with basic research and applications.

All these facts have motivated us to consider the effect of surface anisotropy on the magnetic properties of magnetite nanoparticles. We believe that considering the surface anisotropy as a variable allows us to model different possible scenarios of magnetite nanoparticles embedded in a given matrix or coated by a specific layer. The layout of the article is as follows. In Section II we introduce the model, the Hamiltonian describing the interactions to be considered, some simulation details and the observables to be computed. Numerical results and discussions are presented in Sec. III. This section provides the

temperature dependence of the magnetization and response functions over a wide range of values of the surface-to-core anisotropy ratio. Visualizations of some selected surface spin configurations are presented and discussed. Results are summarized in a proposal of magnetic phase diagram of magnetization and energy as functions of surface anisotropy. A brief discussion about the hysteretic behavior stressing on the core and surface contributions is also addressed. Conclusions are finally presented in Section IV.

## II. MODEL AND SIMULATION

In our model, we simulate the samples by implementing the inverse spinel crystalline structure of magnetite ( $\text{Fe}_3\text{O}_4$ ) with  $Fd\bar{3}m$  symmetry. In this structure, a total number of 56 ions are considered per unit cell. They are distributed as follows: 32  $\text{O}^{2-}$  ions, 8  $\text{Fe}^{3+}$  ions in tetrahedral sites ( $A$ -sites), and finally 8  $\text{Fe}^{2+}$  and 8  $\text{Fe}^{3+}$  ions randomly located in octahedral sites ( $B$ -sites). The iron cations belonging to  $B$ -sites are responsible for the non-resolved sextet observed by Mössbauer spectroscopy above the Verwey temperature. Such a sextet corresponds to a  $\text{Fe}^{2.5+}$  mixed valence state and is a consequence of an electron hopping mechanism between  $\text{Fe}^{2+}$  and  $\text{Fe}^{3+}$  [23]. Thus, the chemical formula can be written as:

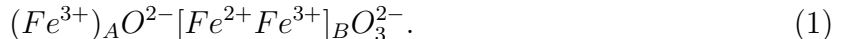


Figure 1 is a graphic representation of the simulated unit cell of magnetite. It also shows the ion distribution, as well as the tetrahedral ( $A$ ) and octahedral ( $B$ ) sites. In the simulation all the iron cation magnetic moments are represented by classical Heisenberg spins. Their magnitudes have been considered by taking into account their respective oxidation states and, therefore, their corresponding electronic configurations. Thus, a value of  $S = 5/2$  was used for  $\text{Fe}^{3+}$  and  $S = 2$  for  $\text{Fe}^{2+}$ . Oxygen ions were considered as non-magnetic. They only favor the occurrence of superexchange interactions. Spins interact via antiferromagnetic couplings when considering the following bonds:  $\text{Fe}_A^{3+}-\text{Fe}_A^{3+}$ ,  $\text{Fe}_A^{3+}-\text{Fe}_B^{3+}$ , and  $\text{Fe}_A^{3+}-\text{Fe}_B^{2+}$ . In contrast, the following couplings are considered ferromagnetic:  $\text{Fe}_B^{3+}-\text{Fe}_B^{3+}$ ,  $\text{Fe}_B^{3+}-\text{Fe}_B^{2+}$ , and  $\text{Fe}_B^{2+}-\text{Fe}_B^{2+}$ . Numerical values of the integrals employed were  $J_{AA} = -0.11$  meV,  $J_{BB} = +0.63$  meV, and  $J_{AB} = -2.92$  meV [24], which were obtained from a first

principles study in the framework of the local spin density approximation (LSDA). Hence, the greater magnitude and sign of the inter-sublattice integral  $J_{AB}$  accounts for anti-parallel inter-sublattice alignment. This fact, in addition to the differences in the spin values, explain the ferrimagnetic behavior observed in bulk magnetite below the Curie temperature. The classical Heisenberg Hamiltonian describing our system can be written as:

$$\begin{aligned} \mathcal{H} = & -2 \sum_{\langle i,j \rangle} J_{ij} \mathbf{S}_i \cdot \mathbf{S}_j - K_V \sum_i (S_{x,i}^2 S_{y,i}^2 + S_{y,i}^2 S_{z,i}^2 \\ & + S_{x,i}^2 S_{z,i}^2) - K_S \sum_k (\mathbf{S}_k \cdot \mathbf{e}_k)^2 - g\mu_B \mathbf{H} \cdot \sum_i \mathbf{S}_i. \end{aligned} \quad (2)$$

The first sum involves all the possible magnetic interactions of iron ions described above and runs over the nearest magnetic neighbors. On this respect it is important to stress that three different nominal coordination numbers under bulk conditions are found for this system, i.e.  $z_{AA} = 4$ ,  $z_{BB} = z_{BA} = 6$ , and  $z_{AB} = 12$ . For instance, the  $z_{AB}$  value indicates that a  $\text{Fe}_A^{3+}$  ion belonging to the core has twelve iron ions belonging to  $B$ -sites. These numbers apply for the core, whereas the surface is defined as formed by those iron ions having smaller coordination numbers. The second term in Eq. (2) is the cubic magnetocrystalline anisotropy and  $K_V$  ( $= 0.002$  meV/spin) is the first-order bulk anisotropy constant [25]. The third term accounts for the surface anisotropy where the unitary vector  $\mathbf{e}_k$  is computed on every  $k$ -th position  $\mathbf{P}_k$ , taking into account the positions  $\mathbf{P}_j$  of the nearest magnetic neighbors [26].

$$\mathbf{e}_k = \frac{\sum_j (\mathbf{P}_k - \mathbf{P}_j)}{\left| \sum_j (\mathbf{P}_k - \mathbf{P}_j) \right|}. \quad (3)$$

Positions over which these vectors were computed correspond exclusively to Fe-cation sites on the surface. The last term in Eq. (2) gives the interaction of spins with a uniform external magnetic field. Estimates of the different energies involved, including dipole-dipole interactions over the entire volume, were initially performed. Such estimates yielded the following orders of magnitude:  $\sim 10^3$  meV/spin for superexchange interactions,  $\sim 10^{-2}$  meV/spin for surface anisotropy,  $\sim 10^{-4}$  meV/spin for cubic anisotropy and  $\sim 10^{-5}$  meV/spin for dipole-dipole interactions. Therefore, dipolar interactions were neglected in the present study [27]. In order to compute equilibrium averages, we have employed a single-spin movement Metropolis-Monte Carlo dynamics. Averages were computed over three different magnetic

starting configurations, and configurational averages were also carried out over 5 different realizations of  $\text{Fe}^{3+}$  and  $\text{Fe}^{2+}$  ions at octahedral sites. Hence, error bars were computed and most of them are smaller than symbol size. A maximum number of  $2.5 \times 10^4$  of Monte Carlo steps per spin (*MCS*) were used and the first  $1.1 \times 10^4$  steps were discarded for equilibration. The lowest temperature considered was 10 K and no special considerations were considered for temperatures below the Verwey temperature,  $T_V$ , known to be at around 120 K for bulk magnetite. The reason for this is experimentally endorsed by several studies in which the suppression of the Verwey transition takes place for particle sizes below 20 nm [25, 28, 29]. For those results giving the dependence with the  $K_S/K_V$  ratio at 10 K, the maximum number of *MCS* was  $5 \times 10^5$  and the first  $2 \times 10^5$  steps were discarded. Numerical values for the  $K_S/K_V$  ratio were taken to range between  $-10^6$  and  $3.5 \times 10^3$ . The analysis of such extreme values allows: i) to determine the stability of the magnetic structures involved and ii) to model different experimental scenarios where a given matrix or a coating medium can effectively change the surface anisotropy. A nearly spherical 5 nm diameter nanoparticle, corresponding to approximately 6 cell parameters along the diameter of the nanoparticle, containing 2731 Fe-ions and 3604 O-ions, was simulated. Hence, 886 Fe-ions belong to the surface, corresponding to 32.4 %. Free boundary conditions were implemented and the thermodynamic quantities computed were energy, magnetization per spin, magnetic susceptibility, and specific heat. Contributions to the total magnetization per magnetic site arising from *A* and *B* sites, from core and shell, as well as for magnetic susceptibility, were explicitly computed. This allows us to monitor the magnetic behavior of the different sublattices and regions.

### III. RESULTS AND DISCUSSION

The temperature dependence of the modulus of the magnetization per spin for  $K_S/K_V = 1$ , including the *A* and *B* contributions, is shown in Fig. 2 for the nanoparticle of 5 nm in diameter. As observed in this figure, the total magnetization lies below the corresponding *A* and *B* contributions, in agreement with a ferrimagnetic state and an anti-parallel inter-sublattice magnetic arrangement. Such an anti-parallel alignment takes place under bulk conditions; the total magnetization per spin goes to a value close to  $2/3$  as the temperature goes to zero. The magnetic susceptibility, shown in the same figure, reveals a maximum

at a critical temperature ( $\sim 801$  K) lower than that of the bulk susceptibility ( $\sim 860$  K). Similarly, the lambda-type behavior of the specific heat shown in Fig. 3, is the typical fingerprint of a thermal driven magnetic phase transition. Temperature values for which response functions exhibit a peak, yield an average estimate of the Curie temperature  $T_C$  at around  $796 \pm 5$  K, which is 64 K lower than that of the bulk. For comparison purposes, results of the specific heat for smaller nanoparticles (3.5 nm and 2.5 nm in diameter) are also shown in Fig. 3. Critical temperature is shifted toward smaller values as the system size decreases. This reduction is ascribed to the lower average magnetic coordination number and, consequently, to the smaller density of magnetic bonds in the nanoparticle compared to those found under bulk conditions. This fact is, in turn, due to the breaking of symmetry on the surface and to an increase in the number of broken exchange bonds. Moreover, the smooth tail of the magnetization at around  $T_C$  is also a typical signal of a finite size effect. More recently, similar finite size effects on  $T_C$  have been reported in maghemite nanoparticles [30].

Regarding the effect of surface anisotropy on the magnetic structure of the nanoparticle, Fig. 4 shows the temperature dependence of the total magnetization per spin for some selected positive  $K_S/K_V$  ratios. The magnetization in the limit of low temperatures decreases as surface anisotropy increases. Such decrease is monotonous below a critical value at around  $\kappa^* \equiv K_S/K_V = 1600$ , above which magnetization drops sharply to a value close to zero. At this value the nanoparticle undergoes a magnetic transition to a spike state characterized by the tendency of the magnetic moments to be almost radially oriented. Anti-parallel alignment between spins of different sublattices is preserved. The onset of this state starts on the surface, where spins tend to follow the single-ion site easy directions imposed by the  $\mathbf{e}_k$  vectors. This configuration is then propagated through the core via superexchange couplings, forcing the core spins to adopt nearly radial orientations. In this manner, the magnetization goes to a value close to zero. Such state corresponds to the lowest energy state and is responsible for the dramatic decrease of magnetization. Snapshots showing surface spin configurations above and below the threshold value  $\kappa^*$  are displayed in Figs. 6 and 5, respectively.

For low  $K_S/K_V$  values, close to one, the spin structure can be considered as a collinear ferrimagnetic state. In this state, all the spins are practically aligned in the same direction, along the easy axis imposed by the core magnetocrystalline anisotropy, and the ferrimag-

netic order is preserved. As the system approaches the threshold value, the spin structure becomes throttled and surface spins begin to adopt outward canted orientations in an attempt to follow those easy directions determined by the  $\mathbf{e}_k$  vectors, while preserving the coupling scheme defined by the superexchange integrals with the inner spins. As a consequence, magnetization slightly decreases. This result agrees with a non-collinear spin structure and with the reduction in the total effective magnetic moment obtained experimentally by ESR measurements in magnetite nanoparticles [6]. It is also important to note that due to its roughness, the surface of the nanoparticle is not strictly spherical and, consequently, easy directions on the surface are not strictly radial, as they have been considered in the so-called transverse surface anisotropy (TSA) models [31, 32]. More concretely, a quenched angular distribution of easy directions, close to a radial geometry, arises instead. Since there are no intermediate easy axes between those imposed by the core cubic anisotropy and those ruled out by the surface, the result is a discontinuity in magnetization. Likewise, the magnetic structure changes in a discontinuous way as the system passes through the critical value  $\kappa^*$ , where the interplay between the two anisotropies becomes more competitive.

Concerning the results at 10 K for negative  $K_S/K_V$  ratios, remarkable differences are found. Instead of having approximately radial easy directions, a distribution of easy planes on the surface is obtained, giving rise to a completely different spin structure. The main feature is the high stability in the magnetization per spin, ranging from around 2/3 down to 0.56 as the absolute value of the  $K_S/K_V$  ratio increases from 1 to such extreme values as  $10^6$ . This means a reduction of 14%, quite different from that obtained for positive  $K_S$  values, whose reduction reaches 95%. Figures 7 and 8 summarize the prior results in a proposal of phase diagram, showing the dependence of both the total magnetization and energy per spin as functions of the  $K_S/K_V$  ratio for positive and negative values, respectively.

Hence, whereas for positive values (Fig. 7) a discontinuous drop in magnetization occurs at the threshold value ( $\sim 1600$ ), for negative values (Fig. 8), a well-behaved and smooth small decrease at around  $|K_S/K_V| = 3000$  takes place. Concerning the energy per spin for positive  $K_S$  values, this exhibits a kink accompanied by a change in the slope at the threshold value, suggesting a finite change in the entropy and the occurrence of a first-order  $K_S$ -driven phase transition. Contrary to this, the energy behaves regularly for negative values of  $K_S$ .

In this last case, the spin structure evolves from a collinear ferrimagnetic single-domain state towards a non-collinear two-pole state above  $|K_S/K_V| = 3000$ , as shown in the snapshot of Fig. 9.

Associated to this spin configuration, high magnetization values are observed. Such state also involves a higher energy cost, as can be evidenced by comparing the energy scale in Figs. 7 and 8. Such a structure, which preserves the local ferrimagnetic order, is in turn consistent with the distribution of easy planes on the surface, which has already been mentioned. In this state, surface magnetic moments tend to be oriented tangential to the surface, whereas the inner most magnetic moments within the core tend to be aligned along the axis defined by the poles. By comparing this configuration with a hypothetical vortex spin structure, it is clear that in the latter, the inner most spins, close to the center of the nanoparticle, would be unable to fulfill the bond configuration ruled out by the superexchange integrals. Contrary to this, in the two-pole configuration, the inner most magnetic moments are highly oriented along the axis defined by the poles and the coupling scheme is easily satisfied.

As for the hysteretic properties, Fig. 10 shows the dependence of the total magnetization per spin and its core and surface contributions as functions of a uniform external magnetic field. Temperature was set at 10 K and  $K_S/K_V=2500$ . Results reveal that, despite the highest applied field (150 T), a fully saturated state was not reached. Such a hard magnetic character is due mainly to surface moments, as can be evidenced in Fig. 10 by the surface contribution. Moreover, despite considering the spike state as the starting spin structure, the nearly radial magnetic configuration is no longer preserved, thereby making the core and surface magnetic moments tend towards a saturation state. When the cycle is performed under the same conditions within a narrower range of field values (minor loop), for which the maxima fields are closer to those found in real experiments, the shape of the loop changes from nearly square to an elongated shape, where the hard magnetic behavior becomes much more evident (Fig. 11). Similar hysteresis loops for ferrimagnetic nanoparticles have been reported through experimental measurements [33] and simulation results [10, 34], where the elongated shapes are ascribed to the occurrence of a surface spin disordered phase. On this respect, it has been argued that the field required to force transitions on surface moments can be very large in ferrite nanoparticles, where the exchange fields can be as large as  $5 \times 10^6$  Oe [3, 5].

The effect of positive and negative surface anisotropy values on the hysteresis is shown in Figs. 12 and 13 respectively. The loop corresponding to bulk magnetite with periodic boundary conditions is included in both figures. Our results show that the switching fields become greater for nanoparticles than for a bulk magnetite at values of  $|K_S/K_V| > 2000$ . Below this value, nanoparticles exhibit lower coercive fields than that of bulk magnetite. Additionally, the coercive force increases with  $|K_S/K_V|$  whereas the remanence decreases (Fig. 14). Such behavior is attributed to a pinning process of the surface spins which becomes more pronounced as the magnitude of the surface anisotropy increases. Thus, as the degree of surface pinning increases, the field required to switch transitions between metastable states is greater. On the other hand, the remanence decreases due to the tendency of the surface magnetic moments to be radially (positive  $K_S$ ) or tangentially (negative  $K_S$ ) oriented, depending on the sign and magnitude of the surface anisotropy constant. Contributions per sublattice to the hysteresis loops were also computed separately. In this case, results revealed the anti-parallel alignment among spins belonging to different sublattices, in agreement with the ferrimagnetic behavior of magnetite. The loops obtained also revealed that the magnetization reversal process, triggered by the external field, occurs concomitantly in both sublattices but with different differential susceptibilities.

Finally, we want to stress that coercive field values obtained through simulation can not be directly compared to those experimentally reported, as long as the coercivity depends on the speed at which the applied field is varied. On this respect, we wish to emphasize that the conditions (MCS and field step) under which the hysteresis loops were recorded remained fixed in all cases. Comparisons are also difficult as far as hysteresis loops for isolated magnetite nanoparticles have to date not been reported, and those found in literature correspond to assemblies of interacting nanoparticles [25].

#### IV. CONCLUSIONS

In conclusion, we have presented simulation results of a core-shell model for magnetite nanoparticles. Our study deals with the different magnetic spin structures that, in principle,

may be found in magnetite nanoparticles under different coating environments, for which different surface anisotropies can be obtained. Our results allow us to conclude a decrease in the Curie temperature, relative to the bulk, as the particle size becomes smaller. Such reduction is attributed to the breaking of symmetry at the surface and, consequently, to a lower density of magnetic bonds. The zero-field magnetic behavior in the low temperature regime shows that the resulting spin structure is strongly influenced by the sign and magnitude of the  $K_S/K_V$  ratio. For positive values of this ratio, above a critical  $\kappa^*$  value at around 1600, magnetization almost vanishes and a non-collinear spike state emerges. In this state, spins tend to be almost radially oriented. Such configuration starts on the surface and then propagates through the core via superexchange couplings. Below this value, a throttled state is visible, in which surface spins become canted with different degrees of orientation and the magnetization slightly decreases with respect to that of the collinear ferrimagnetic single-domain state, observed at small values of  $K_S/K_V$ . Conversely, for negative and extremely high ratios, a two-pole structure evolves. This is characterized by a net magnetization, smaller than that found at low ratios, and agrees with an easy planes distribution on the surface. It must be stressed that, in all cases, the coupling scheme agrees with that of a ferrimagnetic system. Results were finally summarized in a proposal of phase diagram, showing the regimes at which the different spin structures are observed. Hysteresis loops evidenced a magnetically hard behavior, attributed to a pinning phenomenon of surface spins. Coercivity increases as the magnitude of the surface anisotropy increases. In contrast, the remanence decreases due to the tendency of the surface magnetic moments to be radially (positive  $K_S$ ) or tangentially (negative  $K_S$ ) oriented. Finally we expect future experimental evidence to endorse the spin configurations obtained in the present study.

### **Acknowledgments**

This study was supported through the following grants: COLCIENCIAS 1115-05-17603, COLCIENCIAS-CONICYT Colombia-Chile 2005-206, FONDECYT grant 1050066, Millennium Science Nucleus “Basic and applied magnetism” P06-022-F, and the IN1247CE project of Universidad de Antioquia. This work was also partially supported by the Excellence Center for Novel Materials ECNM, under Contract No. 043-2005 subscribed with COLCIENCIAS. One of the authors (J.M.Z) thanks Universidad de Antioquia and COLCIENCIAS

for financial support.

- 
- [1] A. E. Berkowitz, J. A. Lahut, I. S. Jacobs, Lionel M. Levinson, and D. W. Forester, *Phys. Rev. Lett.* **34**, 594 (1975).
- [2] J. M. D. Coey, *Phys. Rev. Lett.* **27**, 1140 (1971).
- [3] D. Lin, A. C. Nunes, C. F. Majkrzak and A. E. Berkowitz, *J. Magn. Magn. Mater.* **145**, 343 (1995).
- [4] A. H. Morr and K. Haneda, *J. Appl. Phys.* **52**, 2496 (1981).
- [5] R. H. Kodama, A. E. Berkowitz, E. J. McNiff Jr., and S. Foner, *Phys. Rev. Lett.* **77**, 394 (1996).
- [6] Yuksel Koseoglu, *J. Magn. Magn. Mater.* **300**, e327 (2006).
- [7] P. Crespo, R. Litrán, T. C. Rojas, M. Multigner, J. M. de la Fuente, J. C. Sánchez-López, M. A. García, A. Hernando, S. Penadés, A. Fernández, *Phys. Rev. Lett.* **93**, 087204 (2004).
- [8] H. Kachkachi and E. Bonet, *Phys. Rev. B* **73**, 224402 (2006).
- [9] D. A. Garanin and H. Kachkachi, *Phys. Rev. Lett.* **90**, 065504 (2003).
- [10] Óscar Iglesias and Amílcar Labarta, *Physica B.* **343**, 286 (2004).
- [11] J. Restrepo, Y. Labaye and J. M. Greneche, *Physica B.* **384**, 221 (2006).
- [12] Laura Hernandez and Claire Pinettes, *J. Magn. Magn. Mater.* **295**, 82 (2005)
- [13] X. Zianni, K. N. Trohidou and J. A. Blackman, *J. Appl. Phys.* **81**, 4739 (1997)
- [14] X. Zianni and K. N. Trohidou, *J. Appl. Phys.* **85**, 1050 (1999)
- [15] O. Nedelko, Slawska-Waniewska, *Phys. Scr.* **T118**, 261 (2005)
- [16] Zhigao Huang, Zhigao Chen, Fengming Zhang, and Youwei Du, *Eur. Phys. J. B* **37**, 177 (2004)
- [17] Z. Huang, Z. Chen, S. Li, Q. Feng, F. Zhang, and Y. Du, *Eur. Phys. J. B* **51**, 65 (2006)
- [18] Franziska Brem, Louis Tiefenauer, Alke Fink, Jon Dobson and Ann M. Hirt, *Phys. Rev. B* **73**, 224427 (2006).
- [19] Hao Zeng, C. T. Black, R. L. Sandstrom, P. M. Rice, C. B. Murray and Shouheng Sun, *Phys. Rev. B* **73**, 020402 (2006).
- [20] Mark Klokkenburg, Ben H. Erné, Johannes D. Meeldijk, Albrecht Wiedenmann, Andrei V. Petukhov, Roel P. A. Dullens and Albert P. Philipse, *Phys. Rev. Lett.* **97**, 185702 (2006).
- [21] D. H. Kim and S. H. Lee and K. H. Im and K. N. Kim and K. M. Kim and I. B. Shim and M. H. Lee and Y.-K. Lee, *Current Appl. Phys.* **6**, e242 (2006).

- [22] Milan Timko, Martina Koneracká, Natália Tomasovicová, Peter Kopcanský and Vlasta Závistová, *J. Magn. Magn. Mater.* **300**, e191 (2006).
- [23] E. De Grave, R. M. Persoons, R. E. Vandenberghe, and P. M. A. de Bakker, *Phys. Rev. B* **47**, 5881 (1993).
- [24] M. Uhl and B. Siberchicot, *J. Phys.: Condens. Matter* **7**, 4227 (1995).
- [25] G. F. Goya, T. S. Berquó, F. C. Fonseca and M. P. Morales, *J. Appl. Phys.* **94**, 3520 (2003).
- [26] R. H. Kodama and A. E. Berkowitz, *Phys. Rev. B* **59**, 6321 (1999).
- [27] H. Kachkachi and M. Dimian, *Phys. Rev. B* **66**, 174419 (2002).
- [28] Jun Wang, Qianwang Chen, Xiaoguang Li, Lei Shi, Zhenmeng Peng and Chuan Zeng, *Chem. Phys. Lett.* **390**, 55 (2004).
- [29] Nicolás A. Fellenz, Sergio G. Marchetti, José F. Bengoa, Roberto C. Mercader and Silvana J. Stewart, *J. Magn. Magn. Mater.* **306**, 30 (2006).
- [30] Óscar Iglesias and Amílcar Labarta, *Phys. Rev. B.* **63**, 184416 (2001).
- [31] R. Yanes, O. Chubykalo-Fesenko, H. Kachkachi, D. A. Garanin, R. Evans, and R. W. Chantrell, *Phys. Rev. B* **76**, 064416 (2007).
- [32] H. Kachkachi and H. Mahboub, *J. Magn. Magn. Mater.* **278**, 334 (2004).
- [33] B. Martínez, X. Obradors, Ll. Balcells, A. Rouanet and C. Monty, *Phys. Rev. Lett.* **80**, 181 (1998).
- [34] Óscar Iglesias and Amílcar Labarta, *J. Magn. Magn. Mater.* **290-291**, 738 (2005).

## FIGURE CAPTIONS

FIG. 1: (Color online) Magnetite unit cell. Gray spheres stand for  $\text{Fe}_A^{3+}$ , blue for  $\text{Fe}_B^{3+}$ , red for  $\text{Fe}_B^{2+}$  and green spheres for oxygen ions. A tetrahedral ( $A$ ) and an octahedral ( $B$ ) site are explicitly drawn.

FIG. 2: (Color online) Magnetization per magnetic site as a function of temperature for the nanoparticle of 5 nm in diameter. Contributions from tetrahedral ( $A$ ) and octahedral ( $B$ ) sites are explicitly shown. The peak position of the magnetic susceptibility reveals a Curie temperature ( $\sim 801$  K) smaller than that of the bulk ( $\sim 860$  K). This feature agrees with the temperature at which the specific heat also exhibits a peak (Fig. 3).

FIG. 3: (Color online) Temperature dependence of the specific heat. A lambda-type behavior is observed, consistent with a thermally-driven ferrimagnetic to paramagnetic phase transition. Positions of the peaks from both the susceptibility (Fig. 2) and the specific heat, give an average estimate of the Curie temperature at around  $796 \pm 5$  K for the 5 nm nanoparticle. Smaller particles yield smaller critical temperatures. Error bars are smaller than symbol size.

FIG. 4: (Color online) Temperature dependence of the total magnetization per spin for the following positive ratios:  $K_S/K_V = 1, 100, 1000, 2000$  and  $3500$ . Error bars are smaller than symbol size.

FIG. 5: (Color online) Surface spin configuration at 10 K for  $K_S/K_V = 1500$  corresponding to the throttled state. Different colors stand for  $\text{Fe}_A^{3+}$  (red),  $\text{Fe}_B^{2+}$  (blue) and  $\text{Fe}_B^{3+}$  (green) surface spins.

FIG. 6: (Color online) Surface spin configuration at 10 K for  $K_S/K_V = 2000$  corresponding to the spike state. Different colors stand for  $\text{Fe}_A^{3+}$  (red),  $\text{Fe}_B^{2+}$  (blue) and  $\text{Fe}_B^{3+}$  (green) surface spins.

FIG. 7: (Color online) Phase diagram: evolution of both the magnetization and energy per spin with the  $K_S/K_V$  ratio for positive  $K_S$  values. Error bars are smaller than symbol size.

FIG. 8: (Color online) Phase diagram: evolution of both the magnetization and energy per spin with the  $K_S/K_V$  ratio for negative  $K_S$  values. Error bars are smaller than symbol size.

FIG. 9: (Color online) Surface spin configuration at 10 K for  $|K_S/K_V| > 3000$  corresponding to the two-pole spin structure. Different colors stand for  $\text{Fe}_A^{3+}$  (red),  $\text{Fe}_B^{2+}$  (blue) and  $\text{Fe}_B^{3+}$  (green) surface spins.

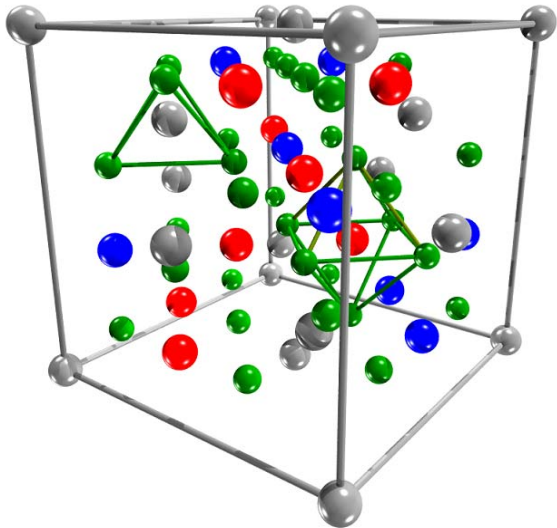
FIG. 10: (Color online) Hysteresis loop at 10 K and  $K_S/K_V=2500$ . Core and surface contributions are explicitly shown.

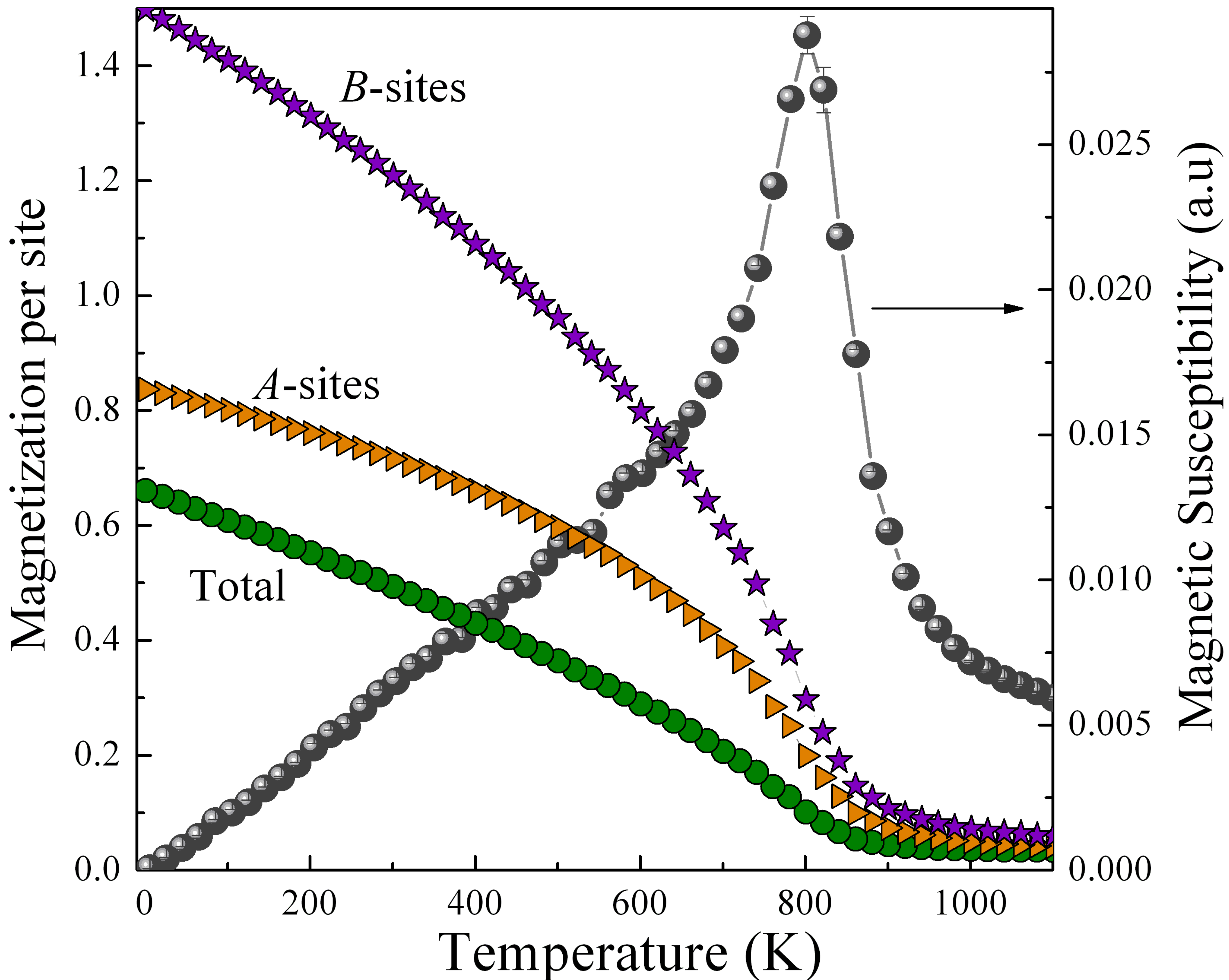
FIG. 11: (Color online) Minor hysteresis loop at 10 K and  $K_S/K_V=2500$  showing the total magnetization per spin as a function of the external applied field.

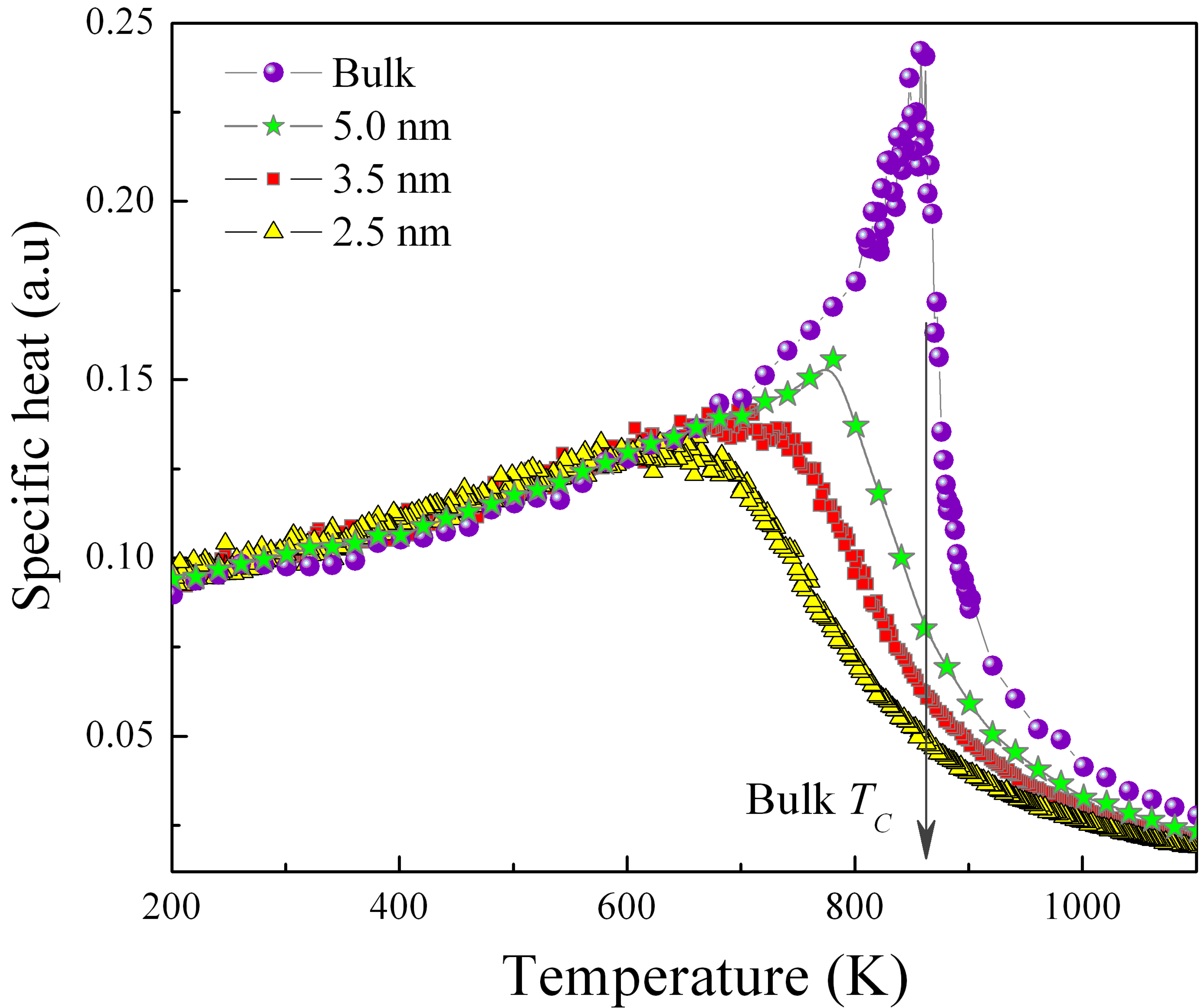
FIG. 12: (Color online) Hysteresis loops at 10 K for  $K_S/K_V=1$  and  $2.5 \times 10^3$ . The loop corresponding to bulk magnetite is also included.

FIG. 13: (Color online) Hysteresis loops at 10 K for  $K_S/K_V=-2.5 \times 10^3$  and  $-2.0 \times 10^5$ . The loop corresponding to bulk magnetite is also included.

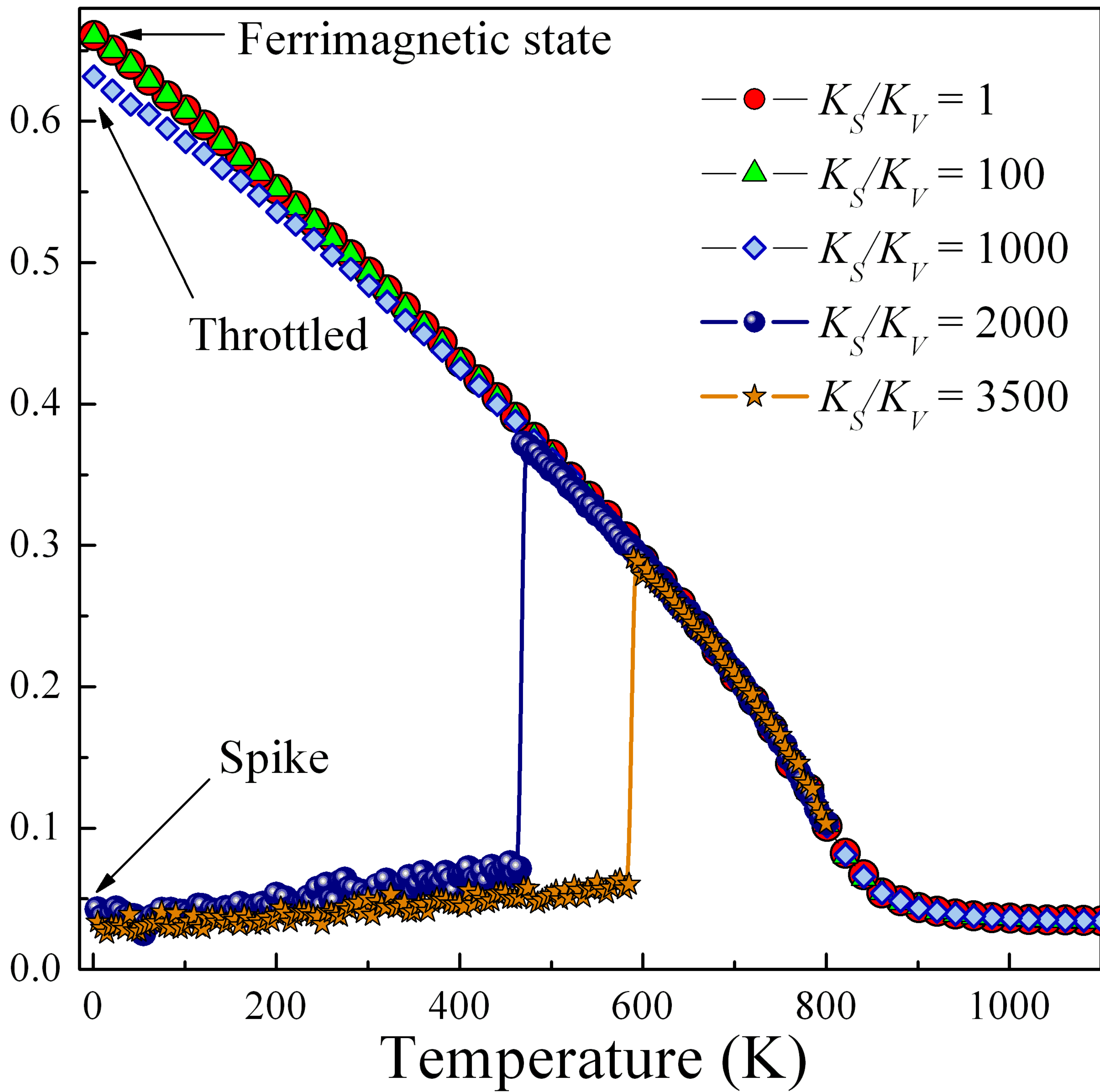
FIG. 14: (Color online) Dependence of both the coercive field and the remanence with the  $K_S/K_V$  ratio.

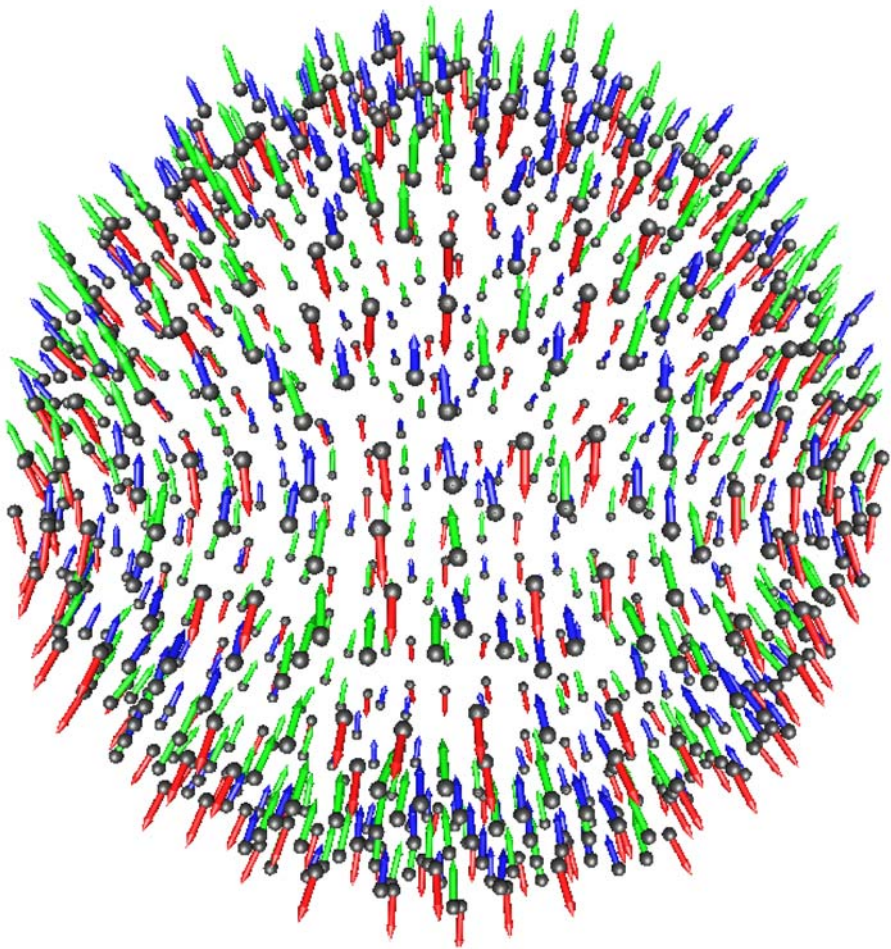


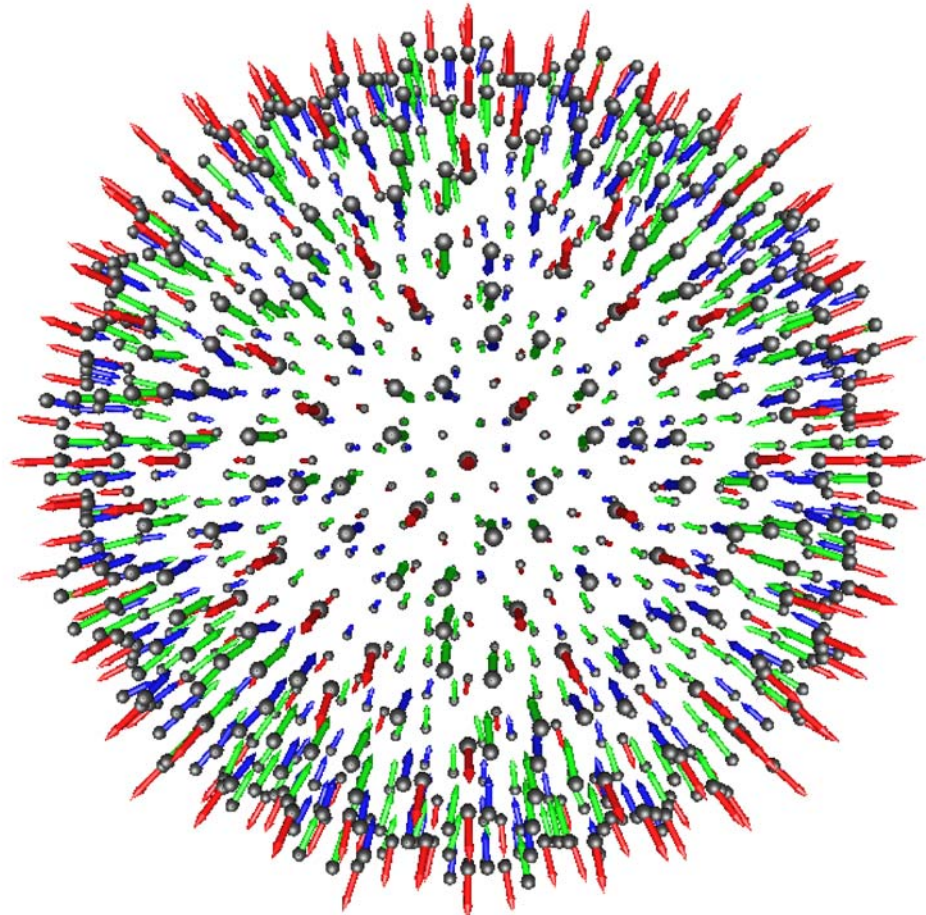


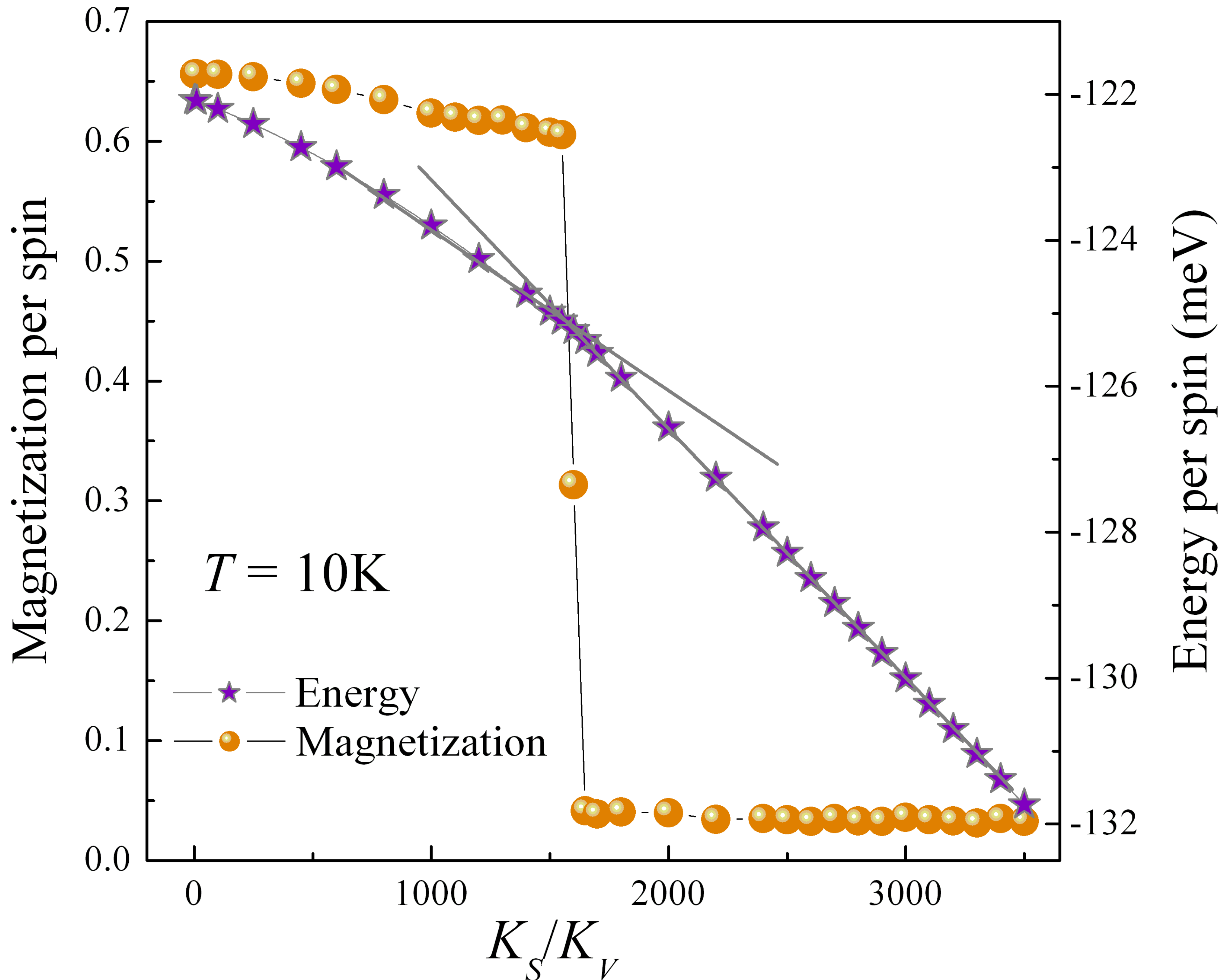


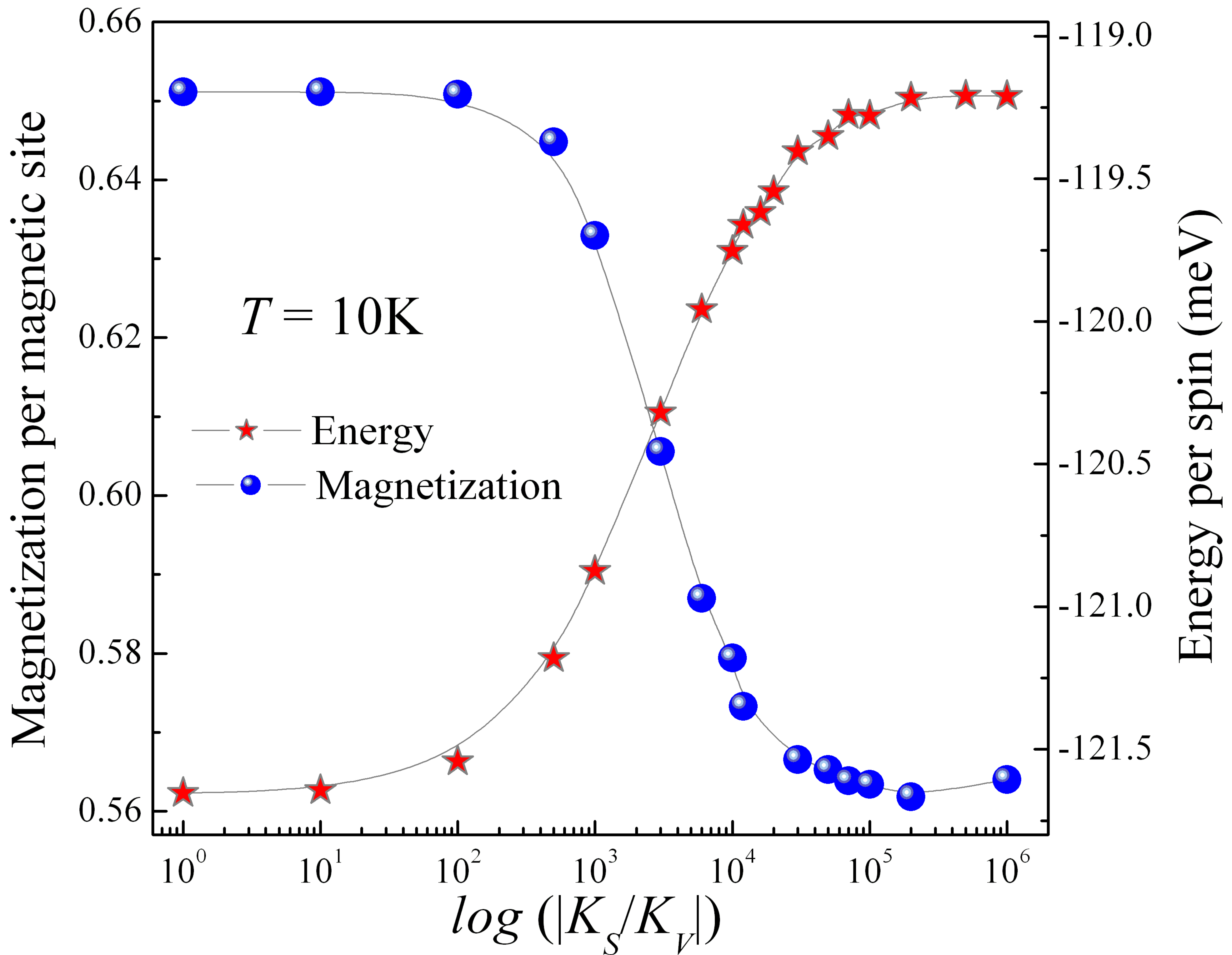
Magnetization per site

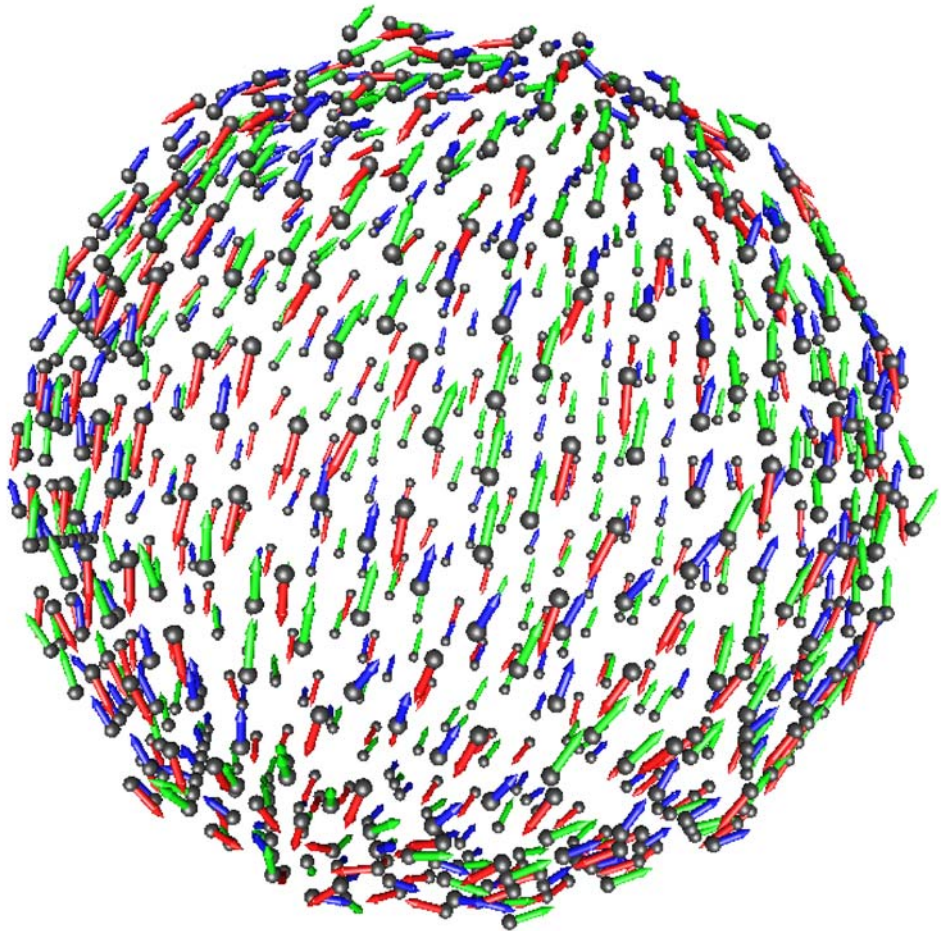


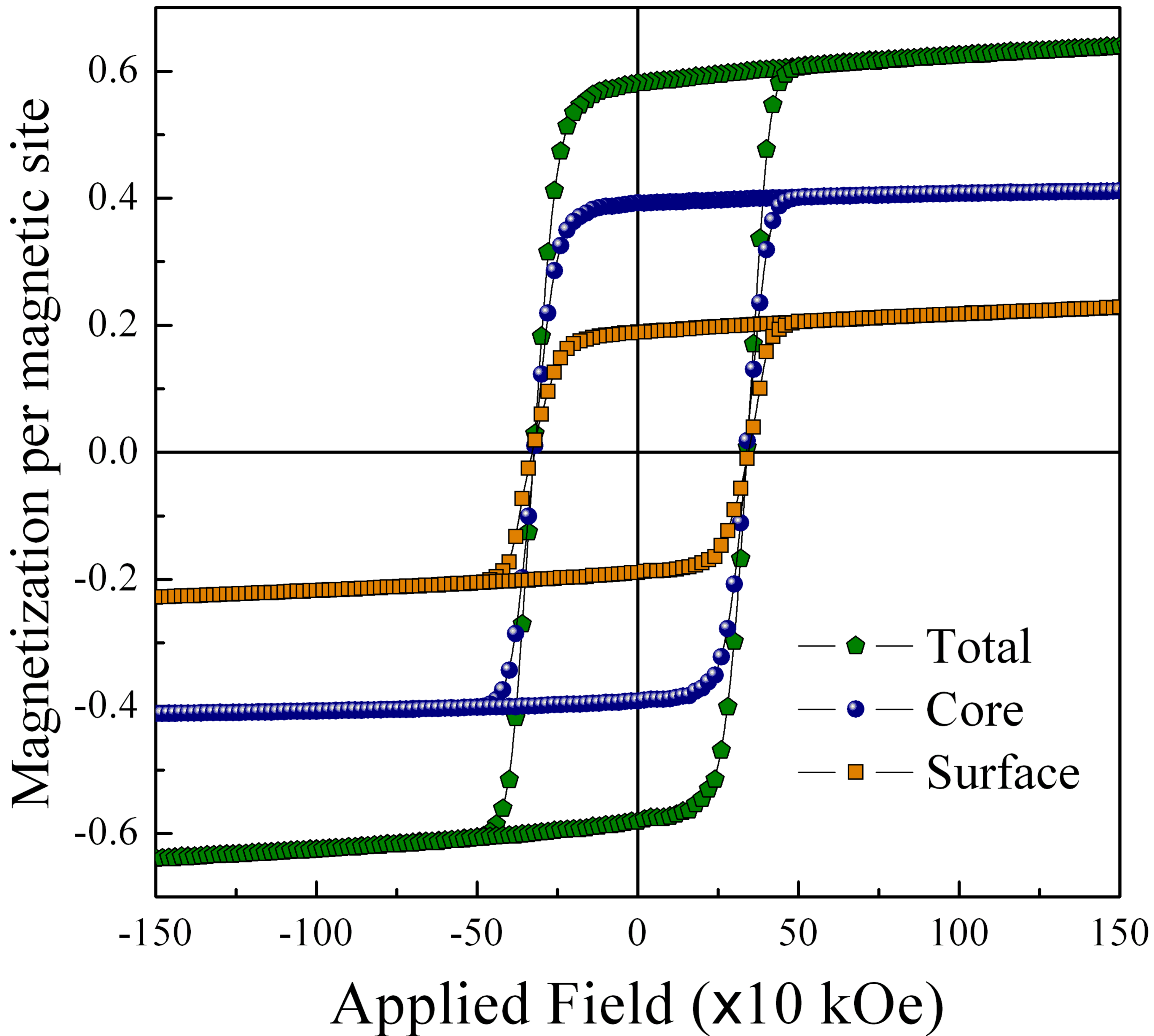




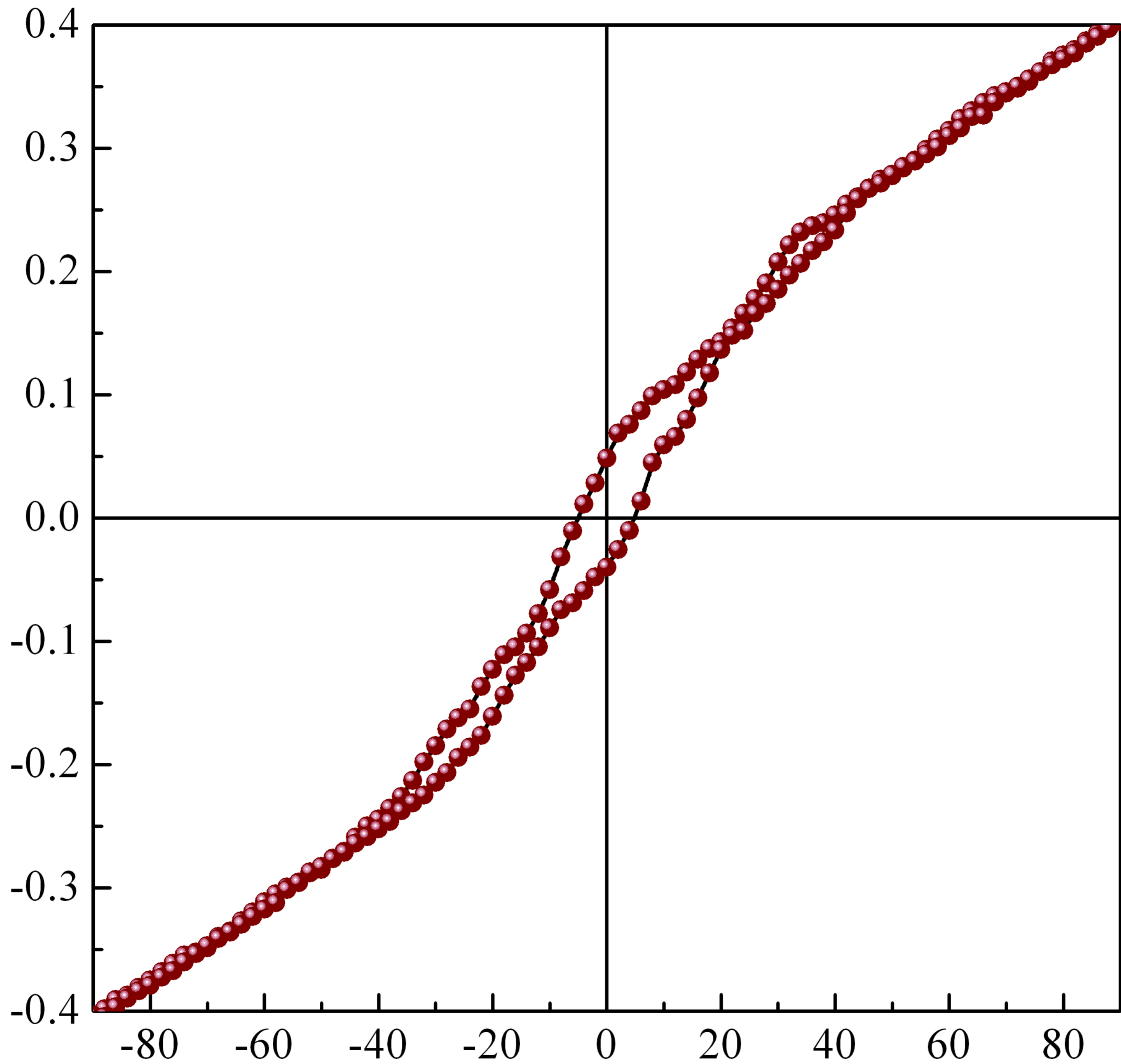








Magnetization per magnetic site



Applied Field (x10 kOe)

